

Revised Conditional t-SNE: Looking Beyond the Nearest Neighbors

Edith Heiter¹, Bo Kang¹, Ruth Seurinck^{1,2}, and Jeffrey Lijffijt¹

¹ Ghent University, Belgium

{edith.heiter,bo.kang,ruth.seurinck,jefrey.lijffijt}@ugent.be

² VIB Center for Inflammation Research, Belgium

Abstract. Conditional t-SNE (ct-SNE) is a recent extension to t-SNE that allows removal of known cluster information from the embedding, to obtain a visualization revealing structure beyond label information. This is useful, for example, when one wants to factor out unwanted differences between a set of classes. We show that ct-SNE fails in many realistic settings, namely if the data is well clustered over the labels in the original high-dimensional space. We introduce a revised method by conditioning the high-dimensional similarities instead of the low-dimensional similarities and storing within- and across-label nearest neighbors separately. This also enables the use of recently proposed speedups for t-SNE, improving the scalability. From experiments on synthetic data, we find that our proposed method resolves the considered problems and improves the embedding quality. On real data containing batch effects, the expected improvement is not always there. We argue revised ct-SNE is preferable overall, given its improved scalability. The results also highlight new open questions, such as how to handle distance variations between clusters.

1 Introduction

Motivation. t-distributed Stochastic Neighbor Embedding (t-SNE) [9] is widely used to compute low-dimensional visualizations for high-dimensional data. Conditional t-SNE (ct-SNE) [3] is an extension of t-SNE that allows to factor out prior knowledge from the embedding. Providing discrete labels for all data points to ct-SNE allows same-labeled points to be embedded further apart than their distances would require—ideally revealing complementary structure present in the data.

We illustrate the idea of conditional t-SNE using a synthetic dataset ($n=1500$, $d=10$) in Figure 1a. The data is generated such that each point belongs to one of two clusters in dim 1-4 (blue, orange) and one of three clusters in dim 5-6 (\circ , \triangle , \square). The remaining four dimensions are Gaussian noise. The t-SNE embedding in 1a shows a separate cluster for each class label combination. If we already know about the clustering in dim 1-4, we could provide the labels blue/orange to ct-SNE. Ideally, this would reveal the remaining structure in the data: Three clusters in dimension 5-6 (\circ , \triangle , \square). Figure 1b shows that ct-SNE wrongly merges the clusters, i.e., \bullet are merged with \blacktriangle , while revised ct-SNE does show the correct clusters (Figure 1c).

Use cases of ct-SNE. (Revised) ct-SNE retains the unsupervised nature of t-SNE while adding supervision through labels to explicate what is *not* the target. This

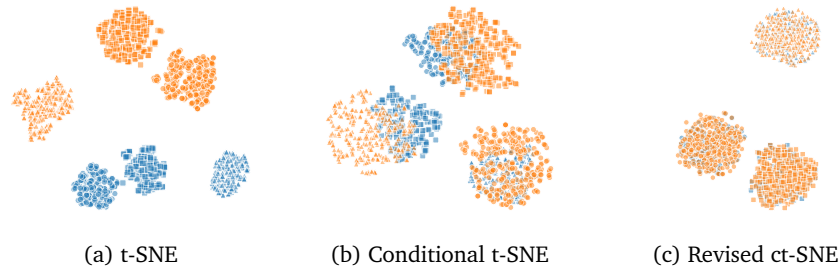


Fig. 1: Illustration of label information used by ct-SNE and revised ct-SNE. (a) t-SNE shows the labeled data consists of several clusters. Provided with the class labels **blue** and **orange**, ct-SNE (b) merges points from both colors—but the wrong shapes, while revised ct-SNE (c) shows the three expected clusters.

stands in contrast to supervised dimensionality reduction methods that incorporate label information to improve downstream prediction tasks, for example by increasing class separation in low-dimensional embeddings (see, e.g., [2, 12]). As such, revised ct-SNE is useful in a situation where t-SNE is useful and when additionally there is known unwanted structure in the data. This may be in an iterative EDA setting, when clusters are identified, explored, and labeled, after which the user wants to explore further. Another setting is when label information about prominent structure in the data is available a priori, and this information acts as a confounder [3].

The presence of undesired and known class separation occurs for example with biological data containing single-cell RNA samples from various sources. The unwanted class separation is called the *batch effect* and can be seen as variation in the data that does not have a biological explanation. It often occurs when combining samples from different organisms, tissues, or when cells have been sequenced with different technologies. For this setting also other t-SNE variants have been proposed. Poličar et al. [10] suggest to embed one dataset (batch) using t-SNE and use this as a reference embedding. The other datasets are then embedded sample by sample on top of the initial embedding. This is different from our (revised) ct-SNE, in that it prevents any interaction of same-labeled samples by design. In addition, (revised) ct-SNE allows the user to tune the degree of class separation.

Contributions. In this paper we provide a thorough analysis of the root cause of ct-SNE’s failures. We identify that the approximation of high-dimensional similarities discards essential structural information. In addition, the asymmetry of the KL-divergence hinders ct-SNE in achieving its goal. To overcome these limitations, we propose two modifications. First, we compute distances for same-labeled and differently-labeled neighbors separately. Second, we condition the high-dimensional instead of the low-dimensional similarities. Finally, we implemented revised ct-SNE into FIt-SNE [6] which leads to a considerable speed-up.

2 Background: Conditional t-SNE

In this section we review ct-SNE and point out details that might negatively affect the embedding quality. The objective of ct-SNE is to embed a dataset $X \in \mathbb{R}^{n \times d}$ to a lower dimension $Y \in \mathbb{R}^{n \times d'}$ with $d' \ll d$ by minimizing the Kullback-Leibler (KL) divergence between pairwise similarities in the high (HD) and low-dimensional (LD) space. The HD similarities

$$p_{j|i} = \frac{\exp(-\|x_i - x_j\|^2 / 2\sigma_i^2)}{\sum_{k \neq i} \exp(-\|x_i - x_k\|^2 / 2\sigma_i^2)}, \quad p_{ij} = \frac{p_{i|j} + p_{j|i}}{2n}$$

are defined with a point-specific kernel bandwidth σ_i that depends on the density of the neighborhood around each point. It is computed by binary search such that each similarity distribution p_i has the same user-defined perplexity u . The LD similarities are based on a t-distribution

$$q_{ij} = \frac{(1 + \|y_i - y_j\|^2)^{-1}}{\sum_{k \neq i} (1 + \|y_k - y_i\|^2)^{-1}}.$$

In ct-SNE, the LD similarities are conditioned on the label matrix $\Delta \in \{0, 1\}^{n \times n}$, based on the idea that $q_{ij|\Delta}$ should be higher for pairs of points with the same label ($\delta_{ij} = 1$) than for points with a different label ($\delta_{ij} = 0$). The conditional LD similarities are defined as

$$r_{ij} = q_{ij|\Delta} = \begin{cases} \alpha q_{ij} / U & \text{if } \delta_{ij} = 1 \\ \beta q_{ij} / U & \text{if } \delta_{ij} = 0 \end{cases}$$

and normalized with $U = \alpha \sum_{k \neq i: \delta_{ki}=1} q_{ki} + \beta \sum_{k \neq i: \delta_{ki}=0} q_{ki}$. We refer to the original publication for the detailed derivation and the exact relationship between the parameters $\alpha > 1 > \beta > 0$. Minimizing $\text{KL}(p \| r)$ with $\alpha > \beta$ requires differently-labeled points to be embedded closer to each other to still match their pairwise HD similarity.

We illustrate the effect of ct-SNE on its gradient

$$\nabla_{y_i} \text{KL}(p \| r) = 4 \sum_{j \neq i} \left(\underbrace{p_{ij} q_{ij} Z(y_i - y_j)}_{\text{attractive force}} - \underbrace{\frac{\delta_{ij} \alpha + (1 - \delta_{ij}) \beta}{U} q_{ij}^2 Z(y_i - y_j)}_{\text{repulsive force}} \right)$$

with $Z = \sum_{k \neq i} (1 + \|y_k - y_i\|^2)^{-1}$. The attractive part will pull neighboring points i and j closer together while the repulsive part pushes all points apart. First, we note that ct-SNE increases (decreases) the repulsive force between same-labeled (differently-labeled) points, while the attractive forces are the same as in t-SNE. To speed up the computation of the attractive forces van der Maaten [8] proposed to exploit the fast decay of the Gaussian kernel and retain only the similarities $p_{\cdot|i}$ for the set of $|\mathcal{N}_i| = 3u$ nearest neighbors, where u is the perplexity.

The problem. The goal of ct-SNE is to bring secondary structure to the front by discounting certain points, i.e., increasing repulsive forces for points with the same

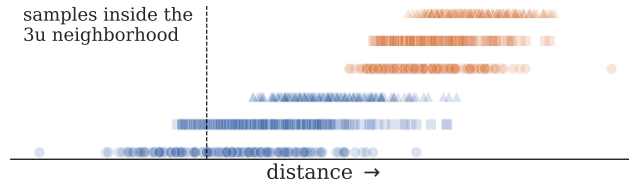


Fig. 2: High-dimensional distances to a random \bullet point aggregated per label. Only samples to the left of the dashed vertical line (all from cluster \bullet or \blacksquare) will exert an attractive force.

label. With a fixed number of $3u$ nearest neighbors—that directly affect the placement of each point—ct-SNE can still only show new structure that reaches into this neighborhood. For the synthetic data, the cluster sizes are larger than $3u$, hence points with different labels are by definition outside the $3u$ neighborhood. In Figure 2 we show the points that are part of \mathcal{N}_{\bullet} . Since the neighbors all have the same blue label, ct-SNE has no information on the similarity to orange labeled points. The overlap between the \bullet and \blacksquare points in Figure 1b occurs solely due to the decreased repulsive forces between differently-labeled samples. It is coincidental and *wrong*, in the sense points from \circ are closer to \bullet , but this information is omitted and a wrong solution emerges (Figure 1b).

Alternative solutions. Increasing the neighborhood size does not lead to the desired results. We explain two ways that seem promising to circumvent the problem but do not work in practice. First, one could keep all pairwise HD similarities instead of approximating them. This results in non-zero attractive forces for differently-labeled points, but increases the complexity to compute these forces in every gradient update to $\mathcal{O}(n^2)$. In addition, the KL-divergence is asymmetric and weighs high p_{ij} to be more important to match with the LD similarity than small similarities. We implemented this method and see in Figure 3a that the embedding on the synthetic data has barely changed. We presume the HD similarities are too small to have an effect on the embedding.

The second idea is to increase the perplexity. A higher perplexity will increase the neighborhood size by definition and differently-labeled neighbors might get assigned a higher similarity than with the first solution (and smaller perplexity). For large datasets with few class labels to be factored out, this might still be impractical, because it could be necessary to use a perplexity of $n/2$ to have sufficiently high attractive forces³. What is even more unfavorable is the loss of *locality* that goes hand in hand with a higher perplexity and stands in opposition with the original idea of t-SNE to preserve local neighborhoods. Figure 3b shows that on the synthetic data a high perplexity indeed leads to better preservation of the similarities between differently-labeled points, but locality is lost and instead two clusters emerge, instead of the expected three clusters.

³ Assuming the distances between differently-labeled samples are larger than between same-labeled samples. A perplexity of $\frac{n}{2}$ would only assign same-labeled points a high similarity.

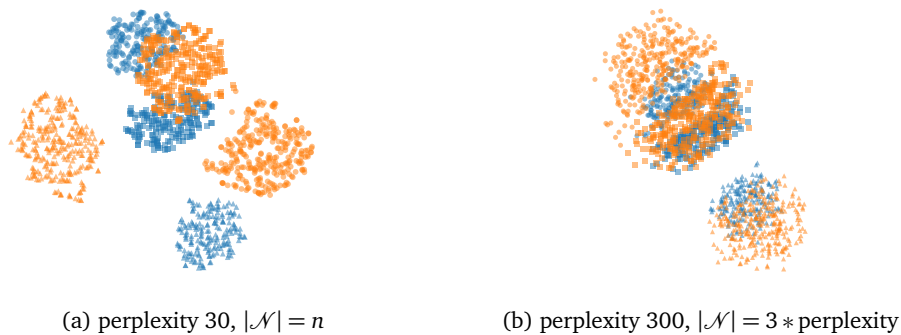


Fig. 3: Visualizations of ct-SNE embeddings ($\beta = 1\text{e-}12$) with color label as prior knowledge. Not approximating the similarities in (a), the clusters still overlap arbitrarily as the attractive forces are too small. A higher perplexity (b) leads to correctly merged clusters that are not well separated. Changing β does not affect the results.

3 Revised Conditional t-SNE

In this section we argue how an adjusted approximation and a different formulation of ct-SNE might help retain important neighborhood information when factoring out prior knowledge. We propose two changes to ct-SNE to provide enough structural information about differently-labeled nearest neighbors and still discount the similarity to same-labeled points.

Expanding the set of nearest neighbors. First, we search for nearest neighbors separately for same and differently-labeled points. We use $\mathcal{N}_{i,\delta_{ij}=1}$ as the set of $1.5u$ nearest neighbors with the same class label as i and $\mathcal{N}_{i,\delta_{ij}=0}$ denotes the set with $1.5u$ differently-labeled nearest neighbors. This does not add runtime to the gradient updates (when still using $3u$ neighbors in total) but requires to build and search in separate nearest-neighbor data structures (e.g., vantage-point trees [13], ANNOY [1]) for each label. As we saw in Figure 3a, this change alone will not be sufficient.

Condition the high-dimensional similarities. The second change is to condition the HD instead of the LD similarities. This will affect the attractive forces, in contrast to the repulsive forces in ct-SNE. We define

$$r_{j|i} = P_{p_i}(j|\Delta) = \frac{P_{p_i}(\Delta|j) \cdot p_{j|i}}{P_{p_i}(\Delta)},$$

where $P_{p_i}(\Delta|j) = \frac{\prod_l n_l!}{n!} \beta^{\delta_{ij}} \alpha^{1-\delta_{ij}}$ is defined as in ct-SNE but we flipped the parameters⁴. The notation P_{p_i} denotes that we compute the similarity distribution for a

⁴ We use α and β instead of α' and β' as in the original paper [3], and thus need to normalize with the number of distinct label assignments.

fixed sample i and the corresponding values of $p_{<.>|i}$. The marginal probability is also defined for each i separately as

$$P_{p_i}(\Delta) = \sum_{k \neq i} P_{p_i}(\Delta|k) \cdot p_{k|i} = \beta \sum_{k \neq i: \delta_{ik}=1} p_{k|i} + \alpha \sum_{k \neq i: \delta_{ik}=0} p_{k|i}.$$

The HD similarities for all samples in the neighborhood are

$$r_{j|i} = \begin{cases} \frac{\beta p_{j|i}}{\beta \sum_{k \neq i: \delta_{ik}=1} p_{k|i} + \alpha \sum_{k \neq i: \delta_{ik}=0} p_{k|i}} & \text{if } j \in \mathcal{N}_{i, \delta_{ij}=1} \\ \frac{\alpha p_{j|i}}{\beta \sum_{k \neq i: \delta_{ik}=1} p_{k|i} + \alpha \sum_{k \neq i: \delta_{ik}=0} p_{k|i}} & \text{if } j \in \mathcal{N}_{i, \delta_{ij}=0}, \end{cases}$$

where the relation between α and β is the same as in ct-SNE, and we will use $\beta < \alpha$ to decrease the similarity of same-labeled data points. Finally, the similarities are symmetrized as before $r_{ij} = (r_{j|i} + r_{i|j})/2n$ and the loss $\text{KL}(r \| q)$ measures the KL-divergence between the conditioned HD similarities and the LD similarities. Since the input similarities do not depend on the embeddings y_i , the gradient is the same as in t-SNE with r_{ij} instead of p_{ij} . This allows us to integrate our changes into FIt-SNE [6] offering a fast interpolation-based acceleration of the gradient computation. Our code is available at github.com/aida-ugent/revised-conditional-t-SNE.

Estimating the point-wise variance. This new formulation of adjusting the HD similarities raises the question whether the point-wise variance of the Gaussian kernel should be computed using r_i or p_i . On r_i , the binary search for the variance satisfying the user-defined perplexity is not well-defined as the perplexity is not monotonously increasing with the variance. Thus, two or more possible solutions exist that can have opposite characteristics as shown in Figure 4. The other option is to first estimate the variance on p_{ij} and then change the similarities with α or β . However, the effective perplexity of r_{ij} might differ from the specified perplexity defined by the user.

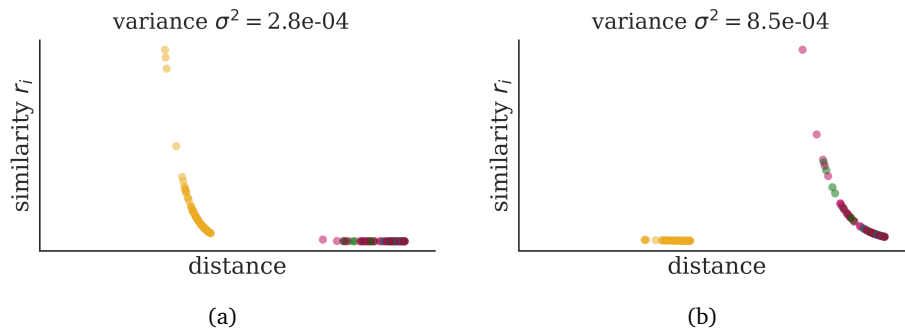


Fig. 4: Two similarity distributions r_i with $\beta = 1e-4$ where a different variance leads to the same perplexity of 50. The distances are computed for cell $i = 12823$ (indrop, beta) of the pancreas dataset and the colors correspond to the technology label.

4 Evaluation

To compare revised ct-SNE with ct-SNE we provide experimental results on a synthetic and two biological datasets. We first describe the evaluation setup including the chosen quality measures and then describe the results. Embeddings of revised ct-SNE with variance estimation on p_i and experimental results on the second biological dataset can be found in the supplement.

4.1 Setup

We first provide the characteristics of the datasets and then define the evaluation measures. All experiments were run on a laptop with Intel® Core™ i7-10850H CPU @ 2.70GHz with 16GB RAM.

Datasets.

Synthetic data Each point in this $n = 1500, d = 10$ dataset belongs to one of two clusters in dimensions 1-4 and one of three clusters in dimensions 5-6. The cluster centers are sampled from $\mathcal{N}(0, 25)$ and $\mathcal{N}(0, 1)$ respectively. For each point, we add noise from $\mathcal{N}(0, 0.01)$ to the cluster centers and append four dimensions of noise from $\mathcal{N}(0, 1)$. The clusters in dim 5-6 are of equal size, while 600 points belong to **blue** and 900 to the **orange** cluster. We provide the cluster labels of dim 1-4 as prior knowledge to ct-SNE and expect the embedding to show the structure implanted in dimensions 5-6.

Pancreas data [11] is a widely-used single cell RNAseq dataset ($n = 14890, d = 34363$) to benchmark data integration methods. It contains gene counts of human pancreatic islets cells from 8 sources sequenced with 5 different technologies—SMARTSeq2 (2394), Fluidigm C1 (638), CelSeq (1004), CelSeq2 (2285), and inDrops (8569). We provide the technology labels as prior knowledge to merge cells from different technologies together and expect a grouping according to the 13 celltypes. We followed the standard preprocessing steps for single-cell RNA datasets including the selection of 2000 highly-variable genes, normalization, standardization, and PCA to retain 50 principal components.

Evaluation measures. To compare the embeddings quantitatively, we compute a normalized HD and LD neighborhood overlap score [4, 5] and the degree of label mixing with the *Laplacian score* that was also used to evaluate ct-SNE. For both measures we use a fixed neighborhood size equal to the perplexity which is 30 for the synthetic and 50 for the pancreas dataset. For the pancreas data, we compute both measures on a random subset of 5% of the data.

R_{NX} neighborhood preservation measures the normalized agreement of HD and LD neighborhoods as proposed by Lee and Verleysen [5]. Denoting the k -sized HD and LD neighborhoods of data point i as v_i^k and n_i^k , the average neighborhood overlap rate is defined as

$$Q_{NX}(k) = \frac{1}{kn} \sum_{i=1}^n |v_i^k \cap n_i^k|.$$

Since a random embedding would yield a score of $\mathbb{E}[Q_{NX}(k)] = \frac{k}{n-1}$, these values are scaled to $R_{NX}(k) = \frac{(n-1)Q_{NX}(k)-k}{n-1-k} \in [0, 1]$, measuring the improvement over a random embedding. We adjust this measure to reflect the idea of factoring out class label information. Given a set of LD neighbors n_i^k , we ensure that v_i^k contains equally many points with the same (and different) label, i.e., $|\{j | j \in v_i^k, \delta_{ij} = 1\}| = |\{j | j \in n_i^k, \delta_{ij} = 1\}|$. The distribution of same and differently labeled neighbors is determined by the embedding and differs per point.

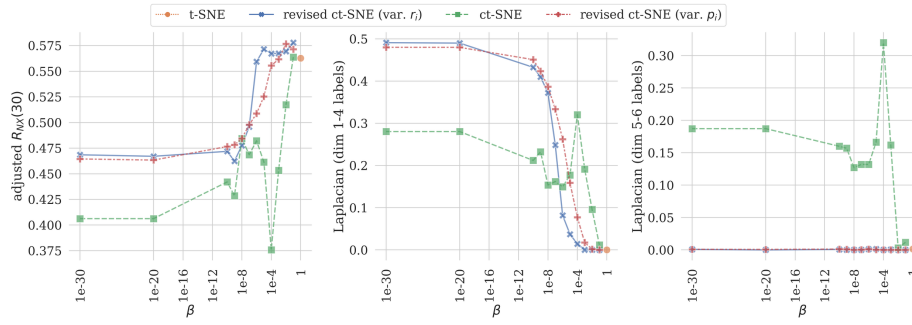
Laplacian scores proposed by Kang et al. [3] measure the fraction of LD nearest neighbors with a different label. It can be compared to a baseline with random label assignment, where the expected Laplacian score is $\sum_{l \in L} \frac{n_l(n-n_l)}{n(n-1)}$ where label $l \in L$ has n_l samples. When factoring out structure encoded by a labeling of the data (e.g. dim 1-4 labels for the synthetic data or the technology feature for pancreas), we expect an increase of the Laplacian score evaluated on the same label. An increase of the Laplacian evaluated on a different class label is not necessarily desirable.

4.2 Results

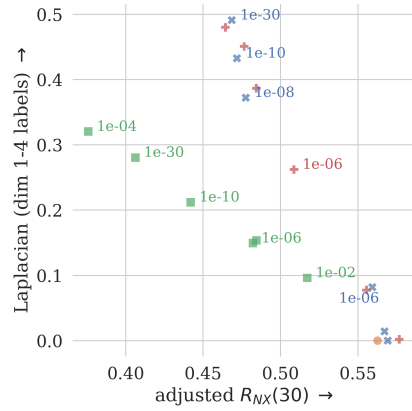
We compare embeddings of t-SNE with embeddings by ct-SNE and revised ct-SNE for different values of β , and using variance estimation with either r_i or p_i .

Synthetic data. To embed the synthetic dataset, we use a perplexity of $u = 30$, $\theta = 0.2$, and 750 epochs. This took about 10s for all methods. The R_{NX} and Laplacian scores are shown in Figure 5 and in Figure 1 we show embeddings of ct-SNE with $\beta = 1e-4$ and revised ct-SNE with $\beta = 1e-20$ as they score highest on the Laplacian (dim 1-4). The t-SNE embedding has a Laplacian score of 0 since the 30 nearest neighbors have the same labels (same color and shape) as we can visually confirm in Figure 1a. Revised ct-SNE converges to a Laplacian score (dim 1-4) equivalent to a random embedding. We conclude that the structure captured by the labels in dimensions 1-4 has successfully been factored out in the embedding. The embedding by ct-SNE scores lower on the Laplacian (dim 1-4 labels) but higher when using the labels in dimensions 5-6 ($\circ, \triangle, \square$). This indicates that not only the imposed structure in dimensions 1-4 but also from dimensions 5-6 has been erroneously removed. The HD neighborhoods for a fixed level of the Laplacian (dim 1-4) are more accurately preserved by revised ct-SNE as shown in in Figure 5b.

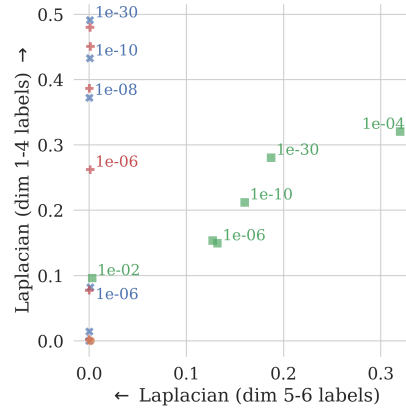
Pancreas data. To embed the pancreas data we use a perplexity of 50, $\theta = 0.5$, and 1000 iterations and show the t-SNE and conditional embeddings with $\beta = 1e-30$ in Figure 6. The runtime of ct-SNE for the pancreas dataset is 168s compared to 28s for revised ct-SNE. The evaluation results depicted in Figure 6a show that the neighborhood agreement $R_{NX}(50)$ drops significantly from 0.44 for t-SNE to 0.30 (ct-SNE) and 0.24 (revised ct-SNE) with $\beta = 1e-30$. Conditional t-SNE and revised ct-SNE both converge to a Laplacian (technology) score that is lower than the score for a random mixing of labels (0.61). The Laplacian for the celltype labels however is high for ct-SNE, indicating a mix of different celltypes in the local neighborhoods.



(a) R_{NX} and Laplacian scores for different values of β evaluated on neighborhoods of size $k = 30$. The t-SNE scores are depicted at $\beta = 1$.



(b) Trade-off between R_{NX} and Laplacian scores based on the dim1-4 labels.

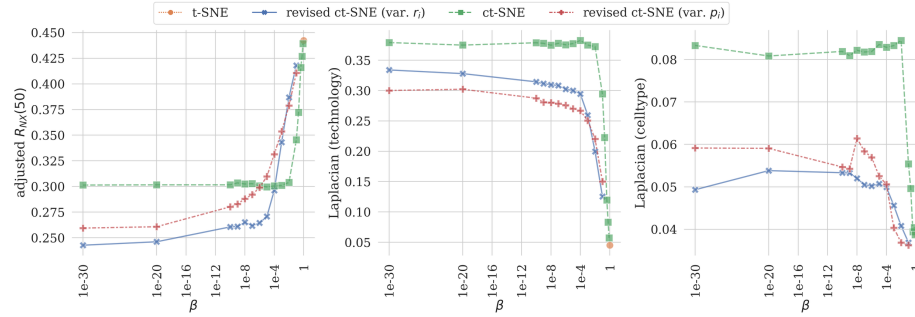


(c) Trade-off between Laplacian scores.

Fig. 5: Evaluation results for the synthetic dataset. In 5a we show the neighborhood agreement and Laplacian for varying β , while 5b and 5c allow to compare two of the measures for a subset of all β values.

Indeed, visualization of the trade-offs (Figures 7a and 7b) learns us that ct-SNE manages to retain R_{NX} better, while mixing the cells from different technologies, whereas revised ct-SNE leads to better trade-offs between the Laplacian scores (less mixing between celltypes, while mixing samples from different batches).

We also notice that $\beta > 1e-4$ is sufficient for ct-SNE while the Laplacian (technology) for revised ct-SNE only plateaus for smaller values of β . We speculate that revised ct-SNE requires smaller values as we change Gaussian HD similarities instead of values from a fat-tailed t-distribution. The trade-offs visualized in Figures 7a and 7b suggest that $\beta = 0.1$ for ct-SNE and $\beta = 1e-4$ for revised ct-SNE might be suitable starting points that can be adjusted in both directions. Finally, the differences in evaluation scores between point-wise variance estimation using r_i and p_i are small and inconclusive.



(a) R_{NX} and Laplacian scores for different values of β evaluated on neighborhoods of size $k = 50$. The t-SNE scores are depicted at $\beta = 1$.

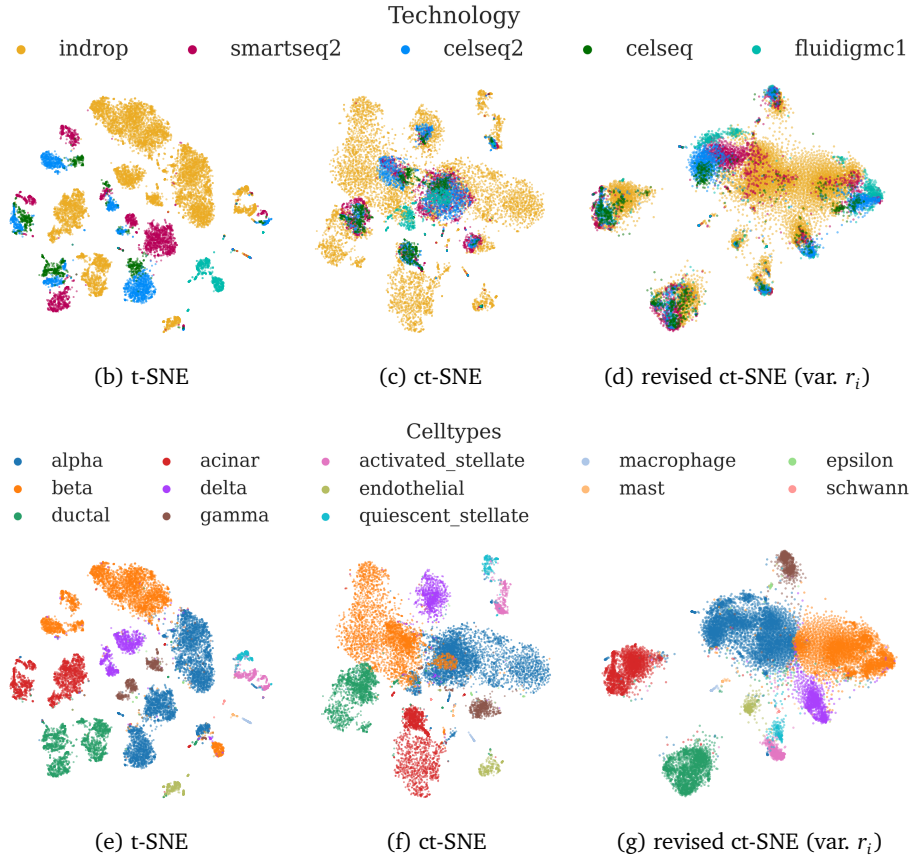


Fig. 6: Visualizations and Laplacian scores of pancreas data embeddings where the technology labels are provided as prior information to ct-SNE and revised ct-SNE with $\beta = 1e-30$. Cell coloring by technology (6b)-(6d) and cell type (6e)-(6g).

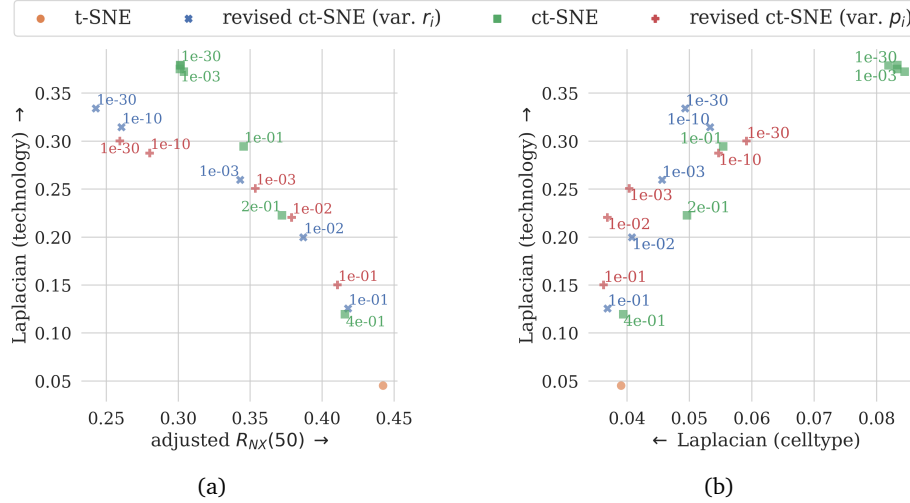


Fig. 7: Evaluation scores for embeddings of the pancreas data. Trade-offs between R_{NX} and Laplacian in (a) and Laplacian technology versus celltype in (b).

5 Discussion

The experiments showed that revised ct-SNE outperformed ct-SNE on the synthetic dataset. On the pancreas dataset, ct-SNE achieved a better trade-off between neighborhood preservation and mixing cells from different technologies, but at the same time in a higher fraction of neighbors with a different celltype. Revised ct-SNE benefits from the Fit-SNE implementation, leading to a faster runtime.

First, we explain the different results of ct-SNE on the two datasets. The original implementation of ct-SNE can suppress a grouping of data points according to given labels, but its ability to reveal larger structures is limited. We showed that the revised formulation avoids *random* placement of points in both the synthetic and the pancreas dataset. The original ct-SNE performs better on the pancreas data than on the synthetic data, because most local neighborhoods also contain cells with a different technology label—which is not the case in the synthetic data. For cells sequenced with ● celseq, there are on average 68 out of 150 nearest neighbors with a different technology label (median 63). However, ● fluidigmc1 cells only have on average 10 out of 150 (median 0) such neighbors. This explains their *almost random* embedding in Figure 6c and 6f where the fluidigmc1, beta cells are mixed with alpha cells and fluidigmc1, alpha cells are mixed with beta cells.

Secondly, we reflect on the two variants of revised ct-SNE where the desired bandwidth of the Gaussian is either estimated on p_i or the final r_i . While the former seems justified for having a unique solution, the *effective* perplexity of r_i can differ from the user-defined perplexity. In the visualizations of the pancreas data (Figures S4 and S5 in the supplement) we noticed circular patterns due to a too small perplexity. We found out that this dataset contains several outlier cells that dominate

the r_i similarity distribution of neighboring cells with a different technology label. We did not observe these patterns when embedding the second biological dataset (Figures S1 and S2).

A final aspect is that revised ct-SNE redefines the similarities with the same β for all labels. If the local HD neighborhood is already mixed with respect to the provided class labels, a larger β might be sufficient. For cells where the distance gap between same and differently-labeled neighbors is large, a smaller β is necessary to reweigh the similarities. In Figure 6 we show the embeddings with $\beta = 1e-30$ which might overshoot the goal for some cells. That means, a too small β can remove the neighborhood information of same-labeled points completely. In summary, neither computing the variance on p_i nor on r_i ensures a stable balance between same and differently-labeled neighbors.

Future Work. Based on the result that revised ct-SNE addresses some shortcomings of ct-SNE but brings a different set of drawbacks, we see various avenues for future work. Firstly we assume that the R_{NX} scores for revised ct-SNE embeddings would increase when the same-labeled similarities do not vanish for small β . Additionally, one could allow for separate *merging strengths* for every label, based on the assumption that all labels should be mixed in the resulting embedding. To ensure a certain trade-off between effective same and differently-labeled neighbors one could compute two separate similarity distributions with two different perplexities. This is a similar idea as implemented in Class-aware t-SNE [2] where the perplexity is adjusted to reach a certain ratio of same-labeled points in the neighborhood. Finally, the embeddings by ct-SNE and revised ct-SNE could be compared to the reference embeddings by Poličar et al. [10] or a combination of data integration methods for biological datasets and t-SNE.

6 Conclusion

We presented revised ct-SNE to find low-dimensional embeddings that show structure beyond a previously known clustering. Conditional t-SNE can fail to reveal this structure when focusing only on the local neighborhoods using small perplexities. To resolve this limitation, we reformulate the original idea to condition the high-dimensional similarities and explicitly include nearest neighbors with different labels. Our experiments on synthetic data confirmed that the revised ct-SNE improved on the criticized aspects of the original method, but ct-SNE performed better in terms of label mixing and neighborhood preservation on real-world single-cell data. Finally, we investigated limitations of revised ct-SNE and proposed to control the number of effective same and differently-labeled neighbors more explicitly.

Acknowledgements The authors would like to thank Tijl De Bie and Yvan Saeys for the discussions about conditional t-SNE. This research was funded by the ERC under the EU’s 7th Framework and H2020 Programmes (ERC Grant Agreement no. 615517 and 963924), the Flemish Government (AI Research Program), and the FWO (project no. 11J2322N, G0F9816N, 3G042220).

Supplement

Revised Conditional t-SNE: Looking Beyond the Nearest Neighbors

Edith Heiter¹, Bo Kang¹, Ruth Seurinck^{1,2}, and Jeffrey Lijffijt¹

¹ Ghent University, Belgium

{edith.heiter,bo.kang,ruth.seurinck,jefrey.lijffijt}@ugent.be

² VIB Center for Inflammation Research, Belgium

1 Human Immune Dataset

The human immune dataset, aggregated by Luecken et al. [7] contains single cell gene expression measurements of $n = 33506$ cells along $d = 12303$ genes. It is a combination of ten batches with cells from five donors, four sequencing technologies and two tissues (peripheral blood and bone marrow). It also includes annotations for 16 different celltypes. We perform the same preprocessing and use their scib[7] package for batch-aware highly-variable gene selection and scaling. Finally, we project the 2000 highly-variable genes to 50 dimensions with PCA.

With ct-SNE [3] and revised ct-SNE, we aim to factor out the differences related to the *batch* labels. For all embeddings we use a perplexity of 50, $\theta = 0.5$, and 1000 iterations. This took about 470 seconds with ct-SNE and 80 seconds with revised ct-SNE (2xIntel(R) Xeon(R) Gold 6136 CPU @ 3.00GHz). The quality was assessed on a subset of 5% of the data (1675 cells) using the adjusted RNX and Laplacian scores.

Table 1: The cells of the datasets were processed using one of three sequencing technologies and stem either from bone marrow or blood samples (PBMC).

batch	technology	tissue
10X	v3_10X	PBMC
Freytag	v2_10X	PBMC
OetjenA	v2_10X	bone marrow
OetjenP	v2_10X	bone marrow
OetjenU	v2_10X	bone marrow
Sun1	10X	PBMC
Sun2	10X	PBMC
Sun3	10X	PBMC
Sun4	10X	PBMC
Villani	smart-seq2	PBMC

In Figures S1 and S2 we show the embeddings of t-SNE, ct-SNE, and revised ct-SNE coloring the cells according to their batch label in the top row and celltype

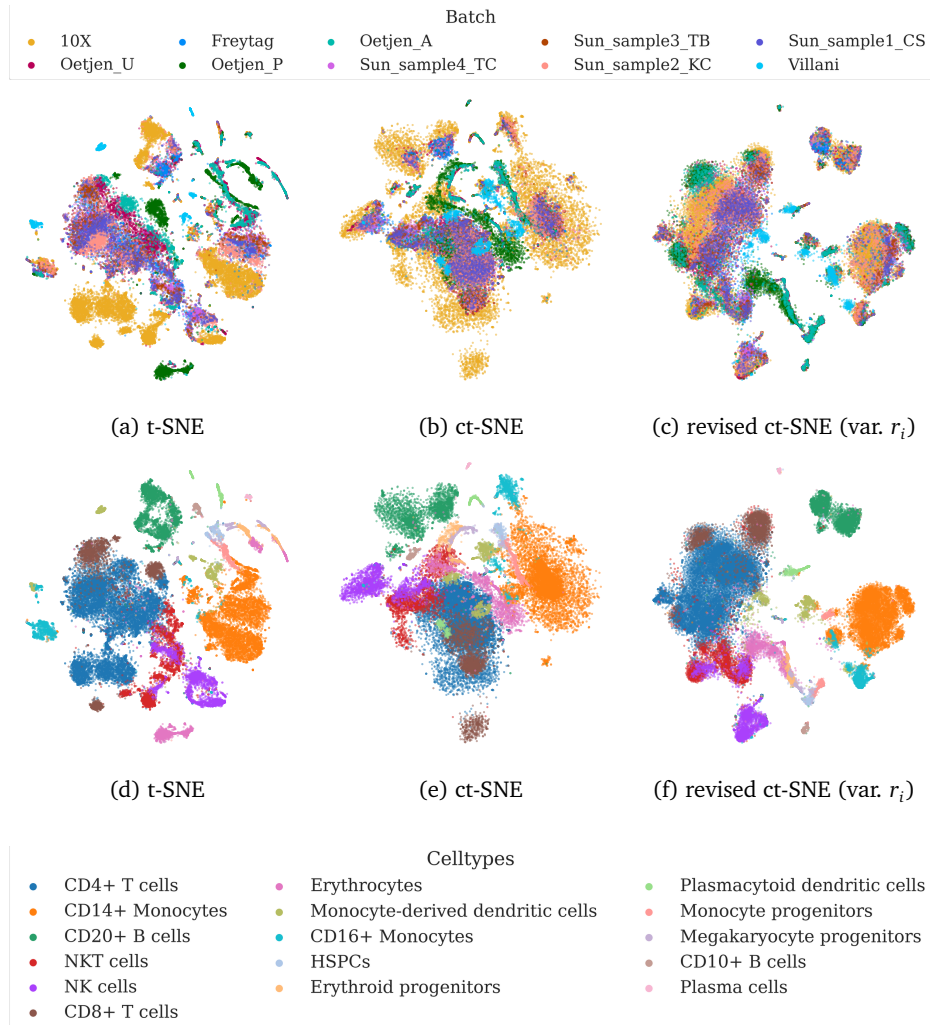


Fig. S1: Visualizations of the Human Immune data where the batch labels are provided as prior information to ct-SNE and revised ct-SNE. For ct-SNE and revised ct-SNE we visualize the embeddings with $\beta = 1e-8$. Cell coloring according to batch (S1a)-(S1c) and celltype (S1d)-(S1f).

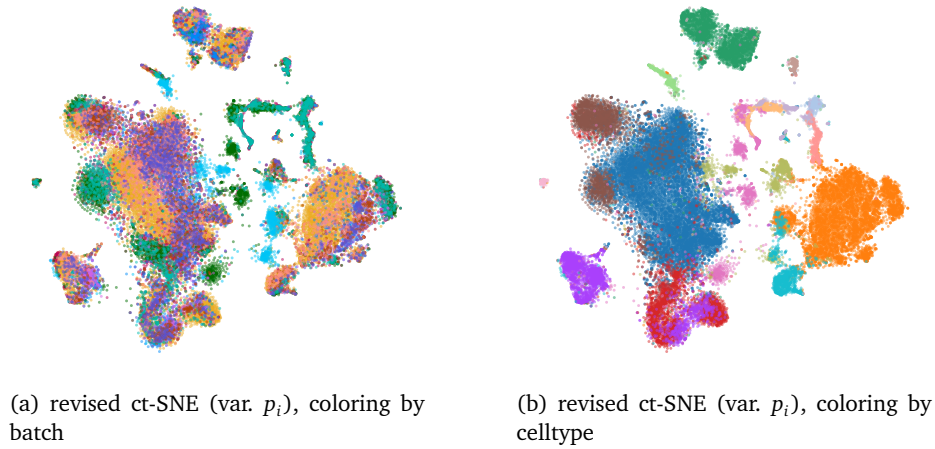


Fig. S2: Embeddings of the immune dataset by revised ct-SNE with variance estimation on p_i

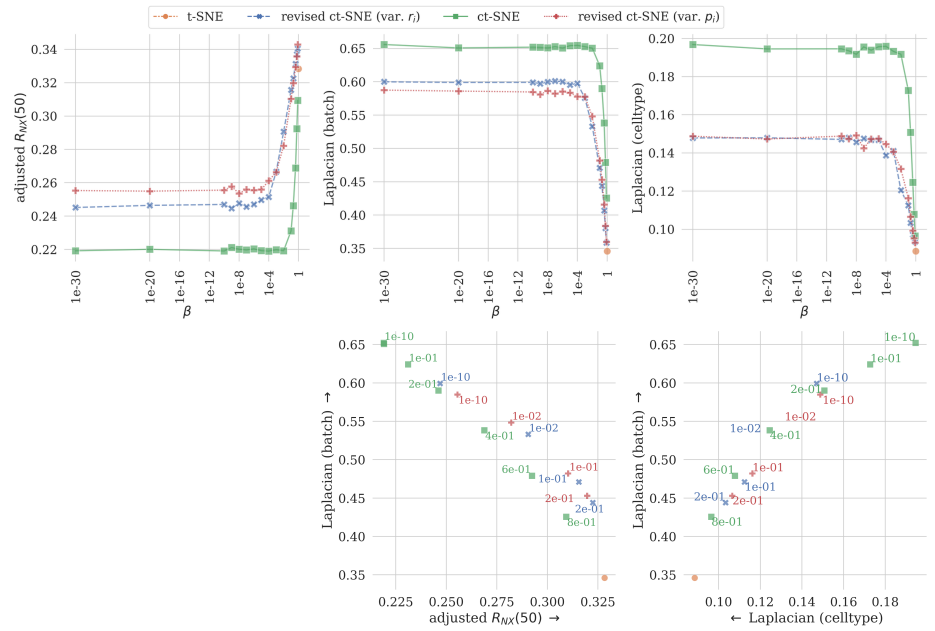


Fig. S3: Human Immune dataset embeddings evaluated with a neighborhood size of $k = 50$. The t-SNE scores are depicted in orange at $\beta = 1$. The first two rows show the trend of the evaluation measures when changing the value for β . The bottom row shows the trade-offs between different evaluation criteria.

in the bottom row. The visualization by t-SNE clearly shows batch effects. Cells from *Villani* and *10X* are separate from all other batches. They were also processed using a different technology (see Table 1). Also cells from *Sun* en *Freytag* cluster together in t-SNE and were sequenced using v2_10X and 10X. The cells from *Oetjen* are also slightly separate from the other batches and are the only ones that stem from bone marrow.

Comparing the embeddings of ct-SNE and revised ct-SNE in Figure S1, we observe that both versions reduce the separation of batches. Revised ct-SNE results in more compact clusters and the coloring according to celltype reveals that ct-SNE results in overlapping celltype clusters. From the evaluation measures in Figure S3 we conclude that ct-SNE is able to merge cells from different batches but does so at the expense of keeping the celltype clusters separate. Revised ct-SNE slightly increases the number of cells with different celltype label in the neighborhood and leads to a better neighborhood preservation for similar Laplacian (batch) values.

2 Pancreas Dataset

To support the analysis of ct-SNE and revised ct-SNE, we analyze the high-dimensional neighborhoods. As ct-SNE is based on the similarity information based on a local neighborhood, we visualize the fraction of neighbors with different technology label in Figures S6 and S7. We note that the indrop cells have very few differently-labeled neighbors which could be the reason of them not being merged with cells from other technologies in the ct-SNE embedding in Figure 6c of the main paper.

We show the revised ct-SNE embedding where the variance is estimated on p_i in Figure S4 and observe several regions with the same pattern as in Figure S5b: For some \bullet indrop cells i , the r_i similarities are dominated by the same \bullet smartseq2 cell j . This smartseq2 outlier has a high similarity $p_{j \cdot | i}$ that only gets larger when the similarity to all differently-labeled points is multiplied with $\alpha > 1$. After re-normalization, all other $r_{\cdot | i}$ will be almost zero and the effective perplexity of r_i is very small.

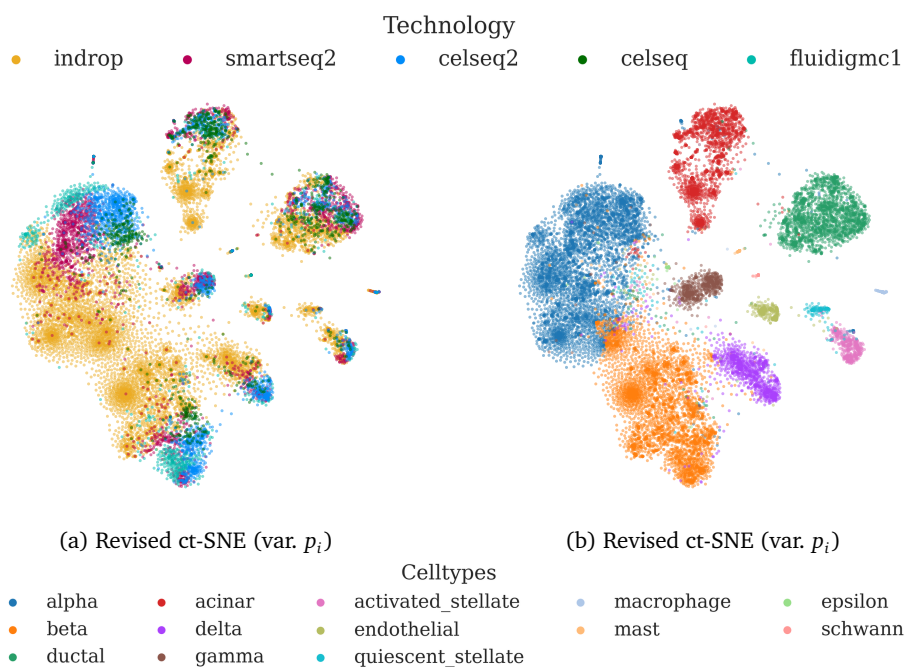
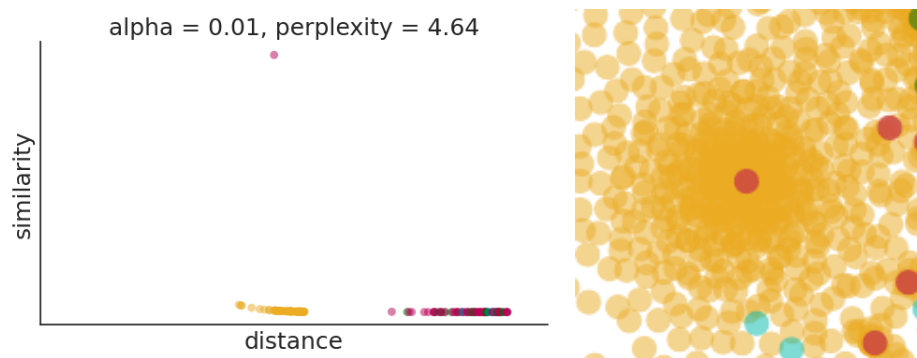


Fig. S4: Embeddings of the pancreas data by revised ct-SNE with variance estimation on p_i .



(a) HD similarities r_i for a \bullet indrop cell when fixing the variance on p_i first. The final similarity distribution r_i has a small perplexity due to the \bullet smartseq2 outlier point in the neighborhood. (b) Embedding structure where many \bullet indrop cells have a high pairwise r_{ij} similarity towards the same \bullet smartseq2 cell.

Fig. S5: Similarity distribution with low perplexity due to outliers in (a) and final embedding of revised ct-SNE (cropped from Figure 4a) in (b).

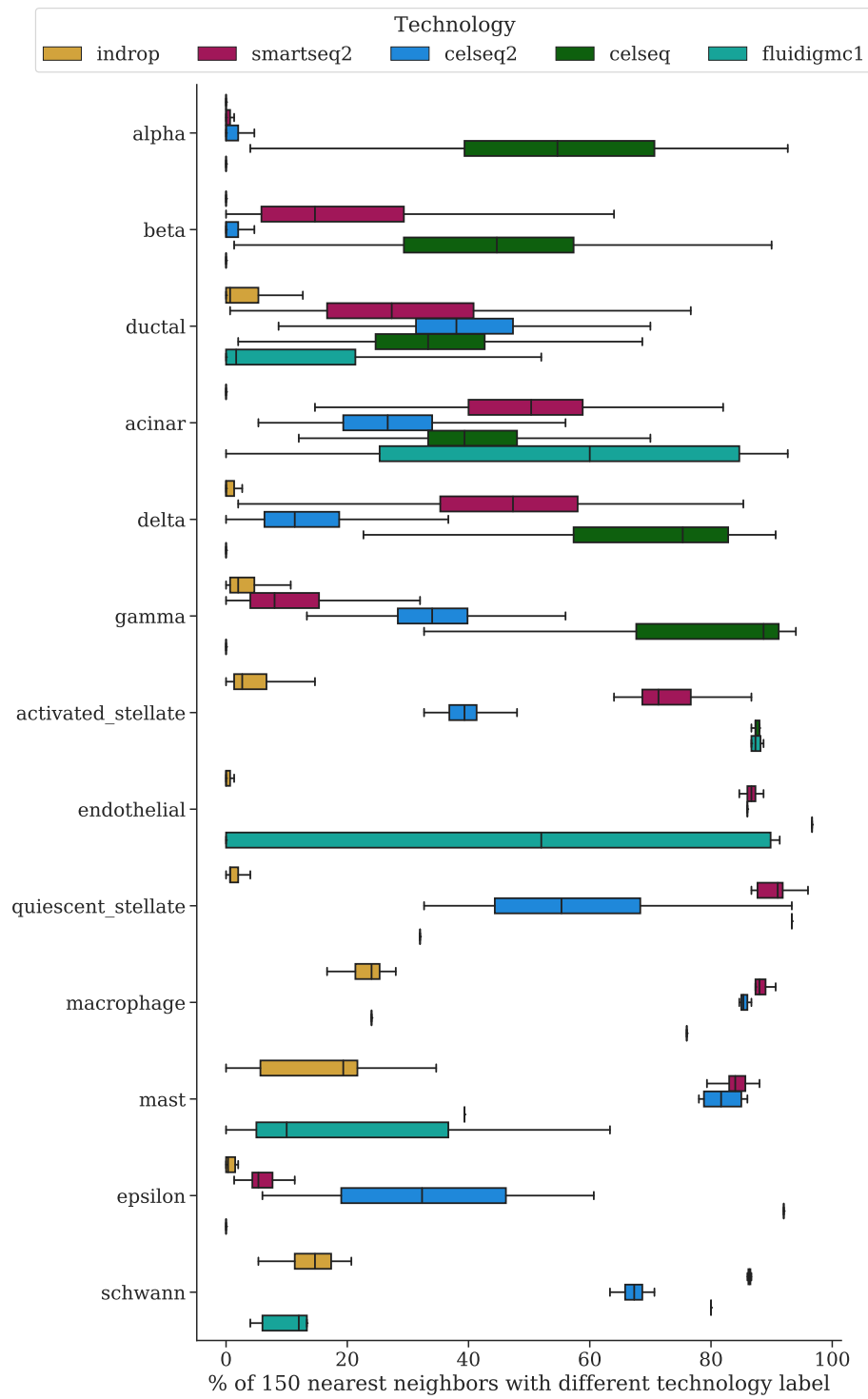


Fig.S6: Boxplots showing the percentage of nearest neighbors in the pancreas dataset with different technology label grouped per celltype and colored by technology. The length of the whiskers is limited to $1.5 \cdot$ interquartile range and we do not show outliers.

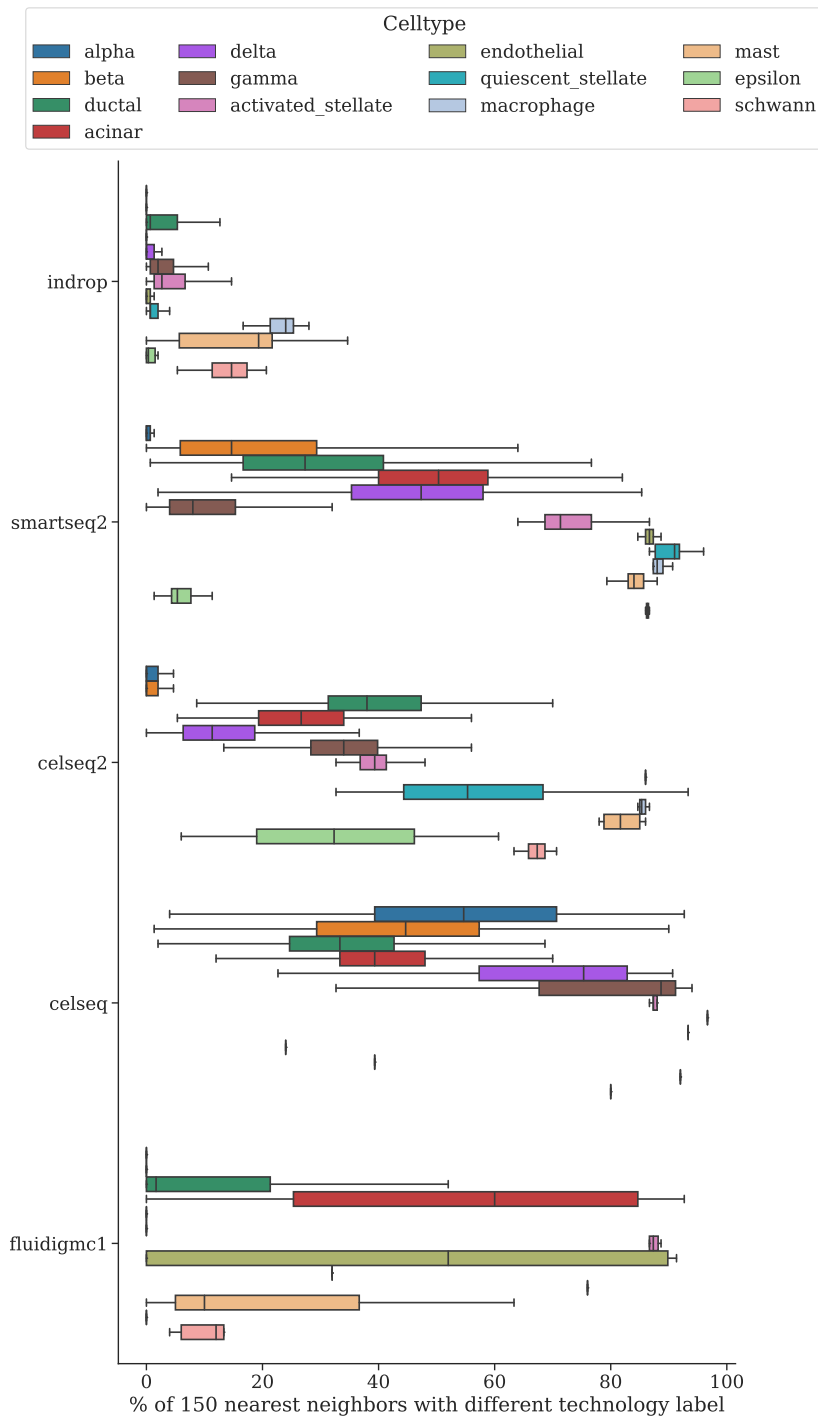


Fig.S7: Boxplots showing the percentage of nearest neighbors in the pancreas dataset with different technology label grouped by technology and colored by cell-type. The length of the whiskers is limited to $1.5 \cdot$ interquartile range and we do not show outliers.

Bibliography

- [1] Bernhardsson, E.: Annoy: Approximate nearest neighbors in c++/python (2013), URL <https://github.com/spotify/annoy>
- [2] de Bodt, C., Mulders, D., Sánchez, D.L., Verleysen, M., Lee, J.A.: Class-aware t-SNE: cat-SNE. In: ESANN (2019)
- [3] Kang, B., García García, D., Lijffijt, J., Santos-Rodríguez, R., De Bie, T.: Conditional t-SNE: more informative t-SNE embeddings. *Machine Learning* **110**(10), 2905–2940 (2021)
- [4] Lee, J.A., Peluffo-Ordóñez, D.H., Verleysen, M.: Multi-scale similarities in stochastic neighbour embedding: Reducing dimensionality while preserving both local and global structure. *Neurocomputing* **169**, 246–261 (2015)
- [5] Lee, J.A., Verleysen, M.: Quality assessment of dimensionality reduction: Rank-based criteria. *Neurocomputing* **72**(7-9), 1431–1443 (2009)
- [6] Linderman, G.C., Rachh, M., Hoskins, J.G., Steinerberger, S., Kluger, Y.: Fast interpolation-based t-SNE for improved visualization of single-cell RNA-seq data. *Nature methods* **16**(3), 243–245 (2019)
- [7] Luecken, M.D., Büttner, M., Chaichoompu, K., Danese, A., Interlandi, M., Müller, M.F., Strobl, D.C., Zappia, L., Dugas, M., Colomé-Tatché, M., et al.: Benchmarking atlas-level data integration in single-cell genomics. *Nature methods* **19**(1), 41–50 (2022)
- [8] van der Maaten, L.: Accelerating t-SNE using tree-based algorithms. *JMLR* **15**(1), 3221–3245 (2014)
- [9] van der Maaten, L., Hinton, G.: Visualizing data using t-SNE. *JMLR* **9**(11) (2008)
- [10] Poličar, P.G., Stražar, M., Zupan, B.: Embedding to reference t-SNE space addresses batch effects in single-cell classification. *Machine Learning* pp. 1–20 (2021)
- [11] Satija Lab: panc8.seuratdata: Eight pancreas datasets across five technologies (2019), R package version 3.0.2
- [12] Vu, V.M., Bibal, A., Frénay, B.: HCt-SNE: Hierarchical constraints with t-SNE. In: International Joint Conference on Neural Networks (IJCNN), pp. 1–8, IEEE (2021)
- [13] Yianilos, P.N.: Data structures and algorithms for nearest neighbor search in general metric spaces. In: Proceedings of ACM-SIAM Symposium on Discrete algorithms, vol. 66, pp. 311–321 (1993)